

# Sensitivity analysis of the chiral magnetic effect observables using a multiphase transport model

Ling Huang,<sup>1,2,3</sup> Mao-Wu Nie,<sup>4</sup> and Guo-Liang Ma<sup>3,1,\*</sup>

<sup>1</sup>*Shanghai Institute of Applied Physics, Chinese Academy of Sciences, Shanghai 201800, China*

<sup>2</sup>*University of Chinese Academy of Sciences, Beijing 100049, China*

<sup>3</sup>*Key Laboratory of Nuclear Physics and Ion-beam Application (MOE),*

*Institute of Modern Physics, Fudan University, Shanghai 200433, China*

<sup>4</sup>*Institute of Frontier and Interdisciplinary Science, Shandong University, Qingdao, 266237, China*

Because the traditional observable of charge-dependent azimuthal correlator  $\gamma$  contains both contributions from the chiral magnetic effect (CME) and its background, a new observable of  $R_{\Psi_m}$  has been recently proposed which is expected to be able to distinguish the CME from the background. In this study, we apply two methods to calculate  $R_{\Psi_m}$  using a multiphase transport model without or with introducing a percentage of CME-induced charge separation. We demonstrate that the shape of final  $R_{\Psi_2}$  distribution is flat for the case without the CME, but concave for that with some amount of the CME. By comparing the responses of  $R_{\Psi_2}$  and  $\gamma$  to the strength of the CME, we show that the CME signal can survive only when the initial charge separation percentage is large enough (more than  $\sim 5\%$ ), which indicates a nonlinear sensitivity of these observables to the CME due to strong final state interactions.

PACS numbers:

## I. INTRODUCTION

Relativistic heavy-ion collisions provide us an unique way to explore the natures of quark gluon plasma(QGP) experimentally [1, 2]. In order to probe the QGP, many observables have been carried out experimentally, such as jet quenching [3–5] and collective flow [6–9]. Recently, the chiral magnetic effect (CME) has been proposed as a good observable which reveals some topological and electromagnetic properties of the QGP. In the early stage of relativistic heavy-ion collisions, an extremely large magnetic field can be created which can induce an electric current along the strong magnetic field for chirality imbalanced domains with a nonzero topological charge inside the QGP, i.e. chiral magnetic effect [10–14]. The transitional observable to detect the CME is a charge-dependent azimuthal correlator,  $\gamma = \langle \cos(\phi_\alpha + \phi_\beta - 2\Psi_{RP}) \rangle$ , which has been widely investigated both experimentally and theoretically [15–21]. Unfortunately, the observable can not distinguish the CME signal from the large background clearly [22–29], because many kinds of backgrounds can contribute to  $\gamma$  similarly as the CME does [25, 27]. Recently, a new observable, namely the shape of  $R_{\Psi_m}$ , has been proposed to be a more sensitive probe to search for the CME signal. Many studies of the  $R_{\Psi_m}$  observable have been reported [30–33]. For examples, some works show that the shape of  $R_{\Psi_m}$  distribution is convex due to background but concave due to the CME [31, 32], but another work shows that  $R_{\Psi_m}$  could be also concave due to the background only [33]. On the other hand, because the lifetime of magnetic field may be quite short due to the limited conductivity of QGP [34–36], it is questionable whether the CME signal formed in the early stage can survive from strong final state interactions since relativistic heavy-ion collisions actually involves many final dynamic evolution stages. It has been found out that a multiphase transport model(AMPT) is a good way to study the interplay between the CME and final state interactions in relativistic heavy-ion collisions [37–39]. Ma et al. [37] demonstrated that a 10% initial charge separation due to the CME can describe experiment data of  $\gamma$  correlator in Au+Au collisions at 200GeV, but only 1-2% percentage of charge separation can remain finally due to strong final state interactions. In this study, we focus on the new observable of  $R_{\Psi_m}$  with two settings of the AMPT models, the original AMPT model which contains backgrounds only and the AMPT model with introducing a CME-induced charge separation. Thus we can compare the change of the shape of  $R_{\Psi_m}$  distribution from the background case to the CME case. We also study the relationship between strength of the CME between  $R_{\Psi_2}$  and  $\gamma$  in order to reveal the sensitivity of those observables to the CME.

This paper is organized as follows. We will introduce our methods of calculating  $R_{\Psi_m}$  and how to introduce a CME-induced charge separation into the AMPT model in Section II. Our results and discussion are presented in Section III.

---

\*glma@fudan.edu.cn

## II. MODEL AND CALCULATION METHOD

### A. The AMPT model

A multiphase transport model, AMPT, has been extensively used to investigate the physics of relativistic heavy-ion collisions [40–45]. In order to study the  $R_{\Psi_m}$ , we simulated Au+Au 200 collisions at 200 GeV (3mb) with the new version of AMPT model with string melting mechanism in which charges are strictly conserved. There are four main stages in the AMPT model [40]: the initial condition, partonic interactions, conversion from partonic to the hadronic matter and hadronic interactions. The initial condition mainly simulates the spatial and momentum distributions of minijet partons from QCD hard processes and soft string excitations by using HIJING model [46, 47]. The parton cascade describes strong interactions among partons through elastic partonic collisions only which are controlled by a partonic interaction cross section [48]. When all partons stop to interact, the AMPT model simulates hadronization by coalescence, i.e. comparing two nearest partons into a meson and three nearest quarks into a baryon. Finally, the ART model is used to simulate baryon-baryon, baryon-meson and meson-meson interactions [49]. There is no the chiral magnetic effect in the original AMPT, so we need to add an additional CME-induced charge separation into the initial condition of the AMPT model in order to study CME-related physics. In previous work [37], the CME signal has been successfully introduced into the AMPT model by switching the  $p_y$  values of a percentage of the downward moving  $u$  ( $\bar{d}$ ) quarks with those of the upward moving  $\bar{u}$  ( $d$ ) quarks to thus produce a charge dipole separation in the initial condition. In our convention, we always choose  $x$  axis along the direction of impact parameter  $b$  from the target center to the projectile center,  $z$  axis along the beam direction, and  $y$  axis perpendicular to the  $x$  and  $z$  directions. The percentage of initial charge separation is used to adjust strength of the CME. The percentage  $f$  is defined as,

$$f = \frac{N_{\uparrow(\downarrow)}^{+(-)} - N_{\downarrow(\uparrow)}^{+(-)}}{N_{\uparrow(\downarrow)}^{+(-)} + N_{\downarrow(\uparrow)}^{+(-)}}, \quad (1)$$

where  $N$  is the number of a given species of quarks,  $+$  and  $-$  denote positive and negative charges, respectively, and  $\uparrow$  and  $\downarrow$  represent the moving directions. By taking advantage of two settings of AMPT model, i.e. without and with introducing the CME, we will apply the new observable  $R_{\Psi_m}(\Delta S)$  to systemically investigate how the new observable works for searching for the CME.

### B. Calculation methods

Two methods, mixing-particle method [30] and shuffling-particle method [31], are used to calculate the new observable of  $R_{\Psi_m}$  for Au+Au collisions at 200GeV (30-50%). Because the definition of  $R_{\Psi_m}$  is based on another observable of  $C_{\Psi_m}$ , we firstly show the formulas for calculating  $C_{\Psi_m}$  in the mixing-particle method as follows [30],

$$\langle S_{p+} \rangle = \frac{1}{N_p} \sum_1^{N_p} \sin\left(\frac{m}{2}(\phi_p^+ - \Psi_m)\right), \quad (2)$$

$$\langle S_{n-} \rangle = \frac{1}{N_n} \sum_1^{N_n} \sin\left(\frac{m}{2}(\phi_n^- - \Psi_m)\right), \quad (3)$$

$$\Delta S = \langle S_{p+} \rangle - \langle S_{n-} \rangle, \quad (4)$$

where  $\phi$  is the azimuthal angle of particle,  $\Psi_m$  is the event reaction plane, superscript  $+$  and  $-$  sign particles' charges,  $N_p$  and  $N_n$  represent the total number of positive and negative charged particles, respectively. For  $m=2$ , the distribution of  $\Delta S$  is expected to be broaden due to the existence of the CME.

In mixing-particle method, to make a corresponding reference of  $\Delta S$ , which is denoted as  $\Delta S_{mix}$ , we select the same number of particles as for  $\Delta S$  but ignore their charges, and we can do similar calculations as follows,

$$\langle S_{p^{mix}} \rangle = \frac{1}{N_p} \sum_1^{N_p} \sin\left(\frac{m}{2}(\phi_p^{mix} - \Psi_m)\right) \quad (5)$$

$$\langle S_{n^{mix}} \rangle = \frac{1}{N_n} \sum_1^{N_n} \sin\left(\frac{m}{2}(\phi_n^{mix} - \Psi_m)\right) \quad (6)$$

$$\Delta S_{mix} = \langle S_{p^{mix}} \rangle - \langle S_{n^{mix}} \rangle. \quad (7)$$

where we use superscript "mix" to sign mixing particles' charges. Then we can get  $C_{\Psi_m}$  by taking the ratio of the distribution of  $\Delta S$  [ $N(\Delta S)$ ] and the distribution of  $\Delta S_{mix}$  [ $N(\Delta S_{mix})$ ].

$$C_{\Psi_m}(\Delta S) = N(\Delta S)/N(\Delta S_{mix}), m = 2, 3 \quad (8)$$

On the other hand, by shifting the  $\Psi_m$  to  $\Psi_m + \pi/m$ ,  $C_{\Psi_m}^\perp(\Delta S)$  is expected to only reflect the background of the CME. We replace  $\Psi_m$  with  $\Psi_m + \pi/m$  in the above formulas,  $C_{\Psi_m}^\perp(\Delta S)$  can be obtained as follows,

$$\langle S_{p^+}^\perp \rangle = \frac{1}{N_p} \sum_1^{N_p} \sin\left(\frac{m}{2}(\phi_p^+ - \Psi_m - \frac{\pi}{m})\right) \quad (9)$$

$$\langle S_{n^-}^\perp \rangle = \frac{1}{N_n} \sum_1^{N_n} \sin\left(\frac{m}{2}(\phi_n^- - \Psi_m - \frac{\pi}{m})\right) \quad (10)$$

$$\Delta S^\perp = \langle S_{p^+}^\perp \rangle - \langle S_{n^-}^\perp \rangle \quad (11)$$

$$\langle S_{p^{mix}}^\perp \rangle = \frac{1}{N_p} \sum_1^{N_p} \sin\left(\frac{m}{2}(\phi_p^{mix} - \Psi_m - \frac{\pi}{m})\right) \quad (12)$$

$$\langle S_{n^{mix}}^\perp \rangle = \frac{1}{N_n} \sum_1^{N_n} \sin\left(\frac{m}{2}(\phi_n^{mix} - \Psi_m - \frac{\pi}{m})\right) \quad (13)$$

$$\Delta S_{mix}^\perp = \langle S_{p^{mix}}^\perp \rangle - \langle S_{n^{mix}}^\perp \rangle \quad (14)$$

$$C_{\Psi_m}^\perp(\Delta S) = N(\Delta S^\perp)/N(\Delta S_{mix}^\perp), m = 2, 3. \quad (15)$$

In the other method of shuffling-particle method, its formulas are same with those of mixing-particle method except for the definitions of  $\Delta S_{mix}$  and  $\Delta S_{mix}^\perp$ . In the above mixing-particle method,  $\Delta S_{mix}$  and  $\Delta S_{mix}^\perp$  are obtained by ignoring charges when mixing all particles. But in shuffling-particle method, they are obtained by reshuffling their charges of charged particles, denoted as  $\Delta S_{shuffle}$  and  $\Delta S_{shuffle}^\perp$ .

For both methods, once we get  $C_{\Psi_m}(\Delta S)$  and  $C_{\Psi_m}^\perp(\Delta S)$ ,  $R_{\Psi_m}(\Delta S)$  [31–33] is obtained as,

$$R_{\Psi_m}(\Delta S) = C_{\Psi_m}(\Delta S)/C_{\Psi_m}^\perp(\Delta S). \quad (16)$$

The shape of  $R_{\Psi_m}(\Delta S)$  is expected to be sensitive to whether the CME exists or not. In our work, we will calculate  $R_{\Psi_m}(\Delta S)$  with the two methods with the AMPT model without and with introducing a CME-induced charge separation, and the detailed results will be presented in the section III.

### III. RESULTS AND DISCUSSIONS

In this work, we selected particles with transverse momenta  $0.35 < p_T < 2.0$  GeV/c and pseudorapidity  $-1.0 < \eta < 1.0$  to calculate  $C_{\Psi_m}$ ,  $C_{\Psi_m}^\perp$  and  $R_{\Psi_m}$ . As for  $\Psi_m$ , the information of coordinate space in the initial stage are used for its reconstruction [50]. Two methods are both applied for calculating  $R_{\Psi_m}$ . The results are presented in subsection IIIA. In order to investigate the relationship between R and the CME strength, the dependence of the CME observables on initial charge separation percentage have been also calculated, which is presented subsection IIIB.

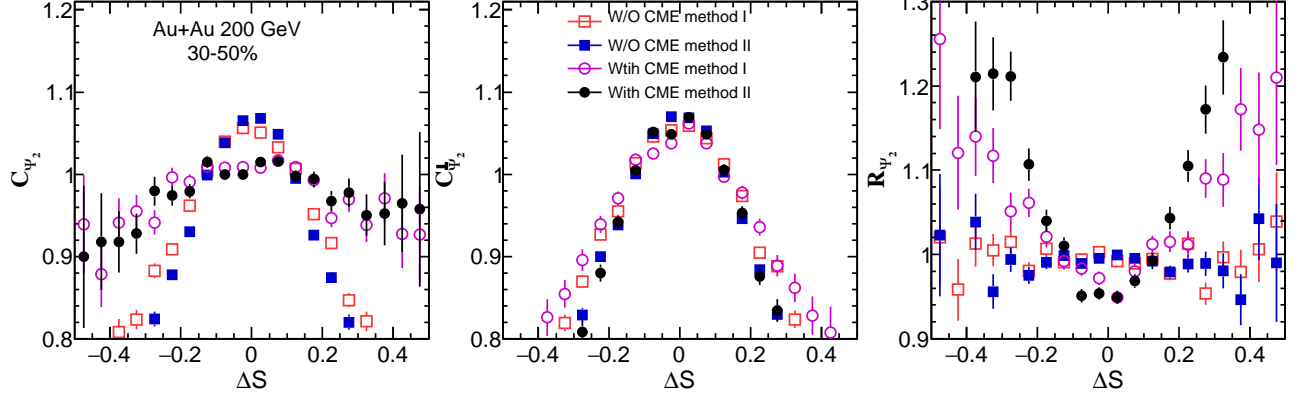


FIG. 1: (Color online)  $C_{\Psi_2}$ ,  $C_{\Psi_2}^{\perp}$  and  $R_{\Psi_2}$  in Au+Au collisions at 200GeV (30-50%) from the AMPT model without or with the CME based on two different methods, where method I and method II represent the mixing-particle method and the shuffling-particle method, respectively.

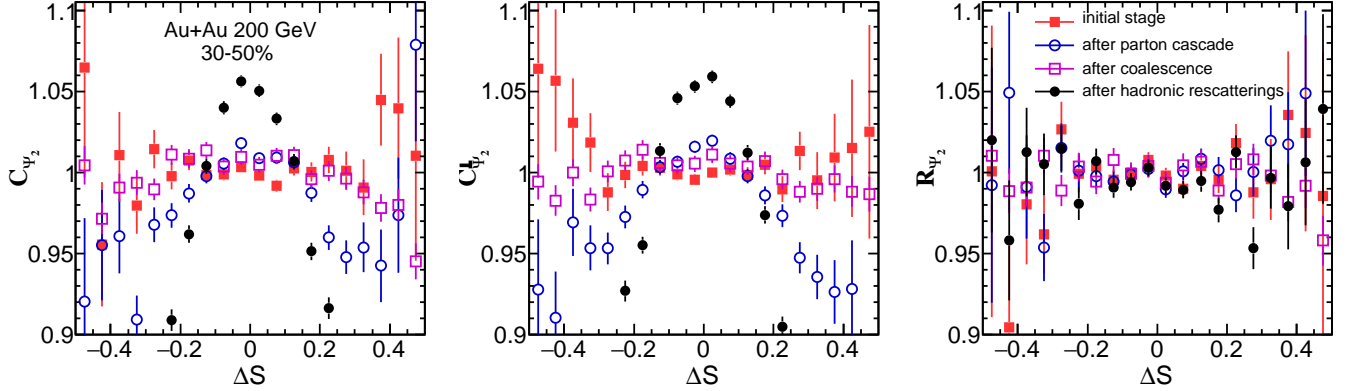


FIG. 2: (Color online)  $C_{\Psi_2}$ ,  $C_{\Psi_2}^{\perp}$  and  $R_{\Psi_2}$  in Au+Au collisions at 200 GeV (30-50%) for different evolution stages of the original AMPT model without the CME.

### A. $C_{\Psi_2}$ , $C_{\Psi_2}^{\perp}$ and $R_{\Psi_2}$

Since the original AMPT model does not include the CME, we can calculate  $R_{\Psi_2}$  through it to study the pure background effect. On the other hand,  $R_{\Psi_2}$  from the AMPT model with introducing the CME can help us find the CME signal from the background. The results are presented in Fig. 1, which shows  $C_{\Psi_2}$ ,  $C_{\Psi_2}^{\perp}$  and  $R_{\Psi_2}$  from the AMPT model without or with introducing an initial CME-induced charge separation based on two methods, where Method I denotes the mixing-particle method and method II denotes the shuffling-particle method. We found that the results from the two methods are consistent with each other. In their shapes,  $C_{\Psi_2}$  and  $C_{\Psi_2}^{\perp}$  are convex for original AMPT model without the CME,  $R_{\Psi_2}$  is flat. On the other hand,  $C_{\Psi_2}$  and  $C_{\Psi_2}^{\perp}$  are convex for the AMPT model with introducing a 10% of CME-induced initial charge separation, but they are broadened differently due to the CME which makes the shape of  $R_{\Psi_2}$  concave finally. From all curves in Fig. 1,  $C_{\Psi_2}$  and  $C_{\Psi_2}^{\perp}$  are convex no matter whether there is the CME or not. However,  $R_{\Psi_2}$  is flat if with background only, but it becomes concave if introducing a 10% of initial CME-induced charge separation.

From the results in Fig. 1, we can see  $R_{\Psi_2}$  can be a probe to distinguish the CME signal from the background. To understand why  $R_{\Psi_2}$  can work for searching for the CME, we further study the stage evolution of  $C_{\Psi_2}$ ,  $C_{\Psi_2}^{\perp}$  and  $R_{\Psi_2}$  for the four stages of heavy-ion collisions in the AMPT model. The results of original AMPT without the CME are presented in Fig. 2. We can see  $C_{\Psi_2}$ ,  $C_{\Psi_2}^{\perp}$  are flat at the initial stage, and then convex at the stage of after parton

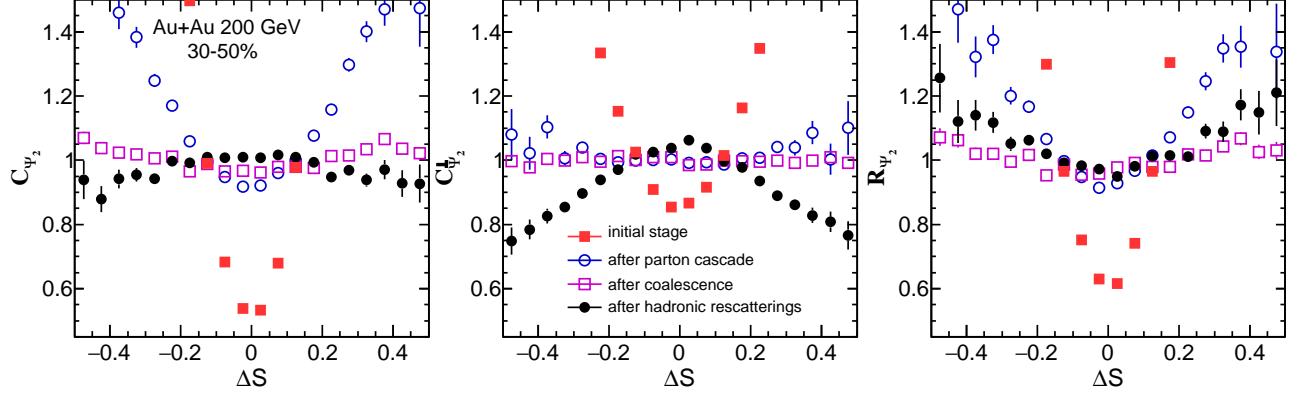


FIG. 3: (Color online)  $C_{\Psi_2}$ ,  $C_{\Psi_2}^\perp$  and  $R_{\Psi_2}$  in Au+Au collisions at 200 GeV (30-50%) from different evolution stages of the AMPT model with a 10% initial CME-induced charge separation.

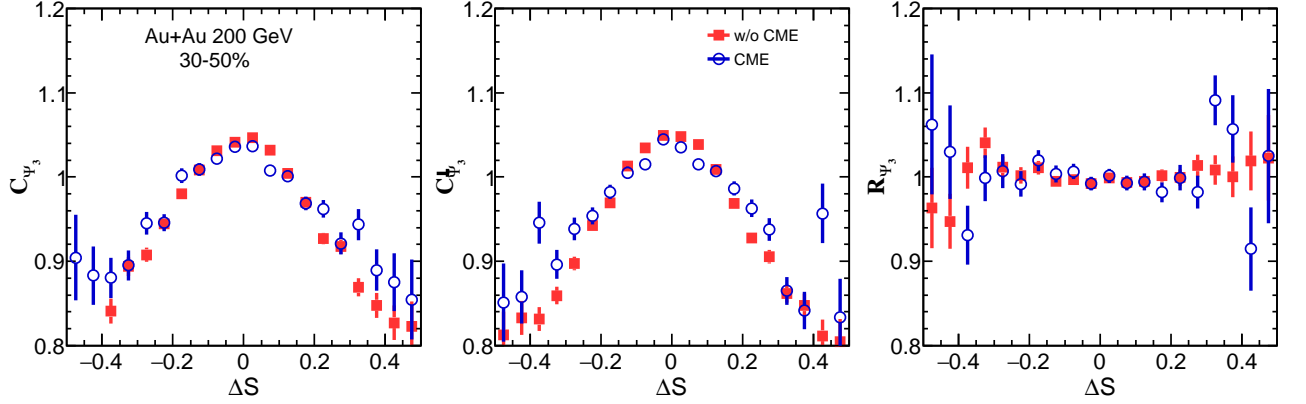


FIG. 4: (Color online)  $C_{\Psi_3}$ ,  $C_{\Psi_3}^\perp$  and  $R_{\Psi_3}$  in Au+Au collisions at 200 GeV (30-50%) from the AMPT model without the CME and with a 10% initial CME-induced charge separation.

cascade. After the coalescence,  $C_{\Psi_2}$  and  $C_{\Psi_2}^\perp$  both trend to be flat, but they become more convex after hadronic rescatterings. However, as the ratio of  $C_{\Psi_2}$  and  $C_{\Psi_2}^\perp$ ,  $R_{\Psi_2}$  is always flat and around the unit from initial stage to after hadronic rescatterings.

At the same time, we also calculated the stage evolution of  $C_{\Psi_2}$ ,  $C_{\Psi_2}^\perp$  and  $R_{\Psi_2}$  for the AMPT model with the CME. As presented in Fig. 3,  $C_{\Psi_2}$ ,  $C_{\Psi_2}^\perp$  and  $R_{\Psi_2}$  are most concave at the initial stage due to introducing the CME. Then after parton cascade, three results are still concave but the magnitude is weakened compared to that at initial stage, due to strong parton cascade. At the stage of after coalescence, three results trend to become flat. After hadronic rescatterings,  $C_{\Psi_2}$  and  $C_{\Psi_2}^\perp$  become convex while  $R_{\Psi_2}$  becomes concave. In this way, the concave shape due to the CME survives from the final state interactions, which gives us a chance to search for the CME by using the new observable of  $R_{\Psi_2}$ . In the previous work, Ma et al. [37] also investigated the evolution of  $\gamma$  observable in the AMPT model which shows final state interactions strongly weaken the initial CME-induced charge separation. Our results indicate that the CME signal from  $R_{\Psi_2}$  is basically consistent with that from the  $\gamma$  observable, i.e. the CME signal from the initial stage is weakened due to final state interactions [37].

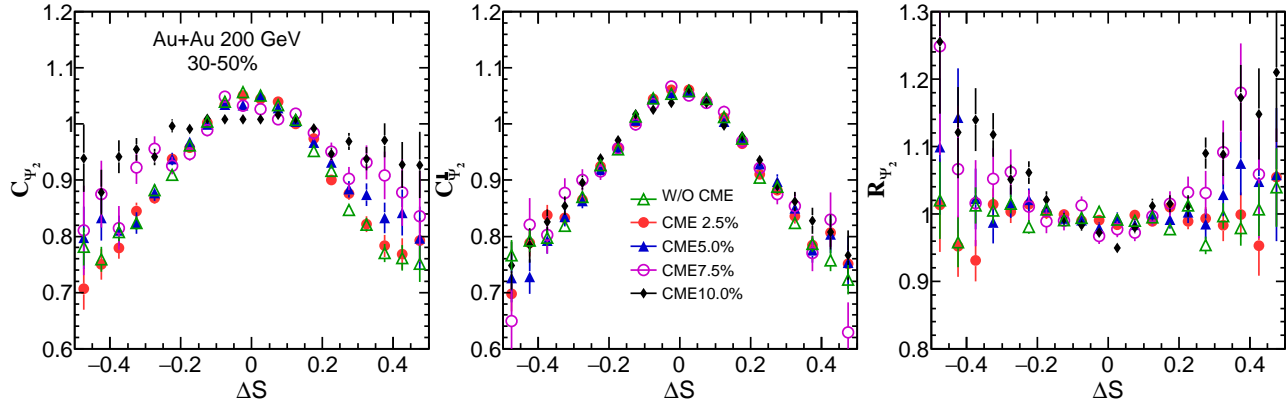


FIG. 5: (Color online)  $C_{\Psi_2}$ ,  $C_{\Psi_2}^\perp$  and  $R_{\Psi_2}$  in Au+Au collisions at 200 GeV (30-50%) from the AMPT model without the CME and with different initial charge separation percentages.

### B. $C_{\Psi_3}$ , $C_{\Psi_3}^\perp$ and $R_{\Psi_3}$

We also study  $R_{\Psi_3}$  which is defined to be respect to the third event plane  $\Psi_3$ . As the direction of magnetic field is expected to be not correlated to  $\Psi_3$ , some research [31] indicates that  $R_{\Psi_3}$  from the background can not identify the CME signal and background. Therefore, we calculated  $R_{\Psi_3}$  for the original AMPT model and the AMPT model with introducing the CME. The results are shown in Fig. 4, we can see that  $C_{\Psi_3}$  and  $C_{\Psi_3}^\perp$  are convex,  $R_{\Psi_3}$  are flat. Because the results from the original AMPT model is same as those from the AMPT model with the CME, which confirms that  $R_{\Psi_3}$  is not sensitive to the CME.

### C. Sensitivity to the CME

In previous work, Ma et al. [37] have studied relationship between the traditional observable of  $\gamma$  and the initial charge separation percentage due to the CME through the AMPT model, which found that  $\gamma$  is not linearly response to the initial charge separation percentage if considering of final state interactions. It demonstrated that only when the charge separation percentage is large enough, e.g. more than 5%, the effect on  $\gamma$  from the CME can become visible. It is interesting to study how sensitive to the CME the new observable of  $R_{\Psi_2}$  is.

Fig. 5 shows the results of  $C_{\Psi_2}$ ,  $C_{\Psi_2}^\perp$  and  $R_{\Psi_2}$  from the AMPT model with different initial charge separation percentages. The results from the original AMPT model without the CME is similar to those from the AMPT model with 2.5% initial charge separation percentage, where  $R_{\Psi_2}$  are both flat within the error bars. When introducing a 5% initial charge separation percentage into the AMPT model,  $C_{\Psi_2}$  become wider than the  $C_{\Psi_2}$  with 2.5% initial charge separation percentage, which makes  $R_{\Psi_2}$  trend to be concave. With the initial charge separation percentage increases, the  $C_{\Psi_2}$  becomes wider and wider, and concave  $R_{\Psi_2}$  becomes narrower and narrower. These results indicate that  $R_{\Psi_2}$  is insensitive to the CME if the initial charge separation percentage is below 5%. When the initial charge separation percentage is larger than 5%, the shape of  $R_{\Psi_2}$  becomes sensitive to the CME.

In order to compare the sensitivities to the CME between  $\gamma$  and R, we study how they depend on the initial charge separation percentage. In the left plot of Fig. 6, we show that the  $\gamma$  and  $\Delta\gamma$  have a nonlinear response to the initial charge separation percentage. The  $\gamma$  and  $\Delta\gamma$  from the AMPT with a 2.5% initial charge separation percentage is same as those from the original AMPT model (0%).  $\gamma$  and  $\Delta\gamma$  from the AMPT model with a 5.0% initial charge separation percentage is slightly different from those with 0% and 2.5% initial charge separation percentages, which indicates it is difficult for using  $\gamma$  to detect the CME if the initial charge separation percentage is less than 5.0%. When the initial charge separation percentage increases from 5% to 10%, the  $\gamma$  and  $\Delta\gamma$  start to increase with the initial charge separation percentage, which is consistent with the previous results from Ma et al. [37]. On the other hand, the right plot of Fig. 6 shows the width of  $C_{\Psi_2}$ ,  $C_{\Psi_2}^\perp$  and  $R_{\Psi_2}$  distributions for different initial charge separation percentages in Au+Au collisions (30-50%), where we apply a Gaussian function to fit the distributions of  $C_{\Psi_2}$ ,  $C_{\Psi_2}^\perp$  and  $R_{\Psi_2}$ . We can see that the width of  $C_{\Psi_2}$  increases but  $C_{\Psi_2}^\perp$  changes little, so the width of  $R_{\Psi_2}$  decreases, but only when the initial charge separation percentage increases from 5%. Through the comparison, our results indicate that

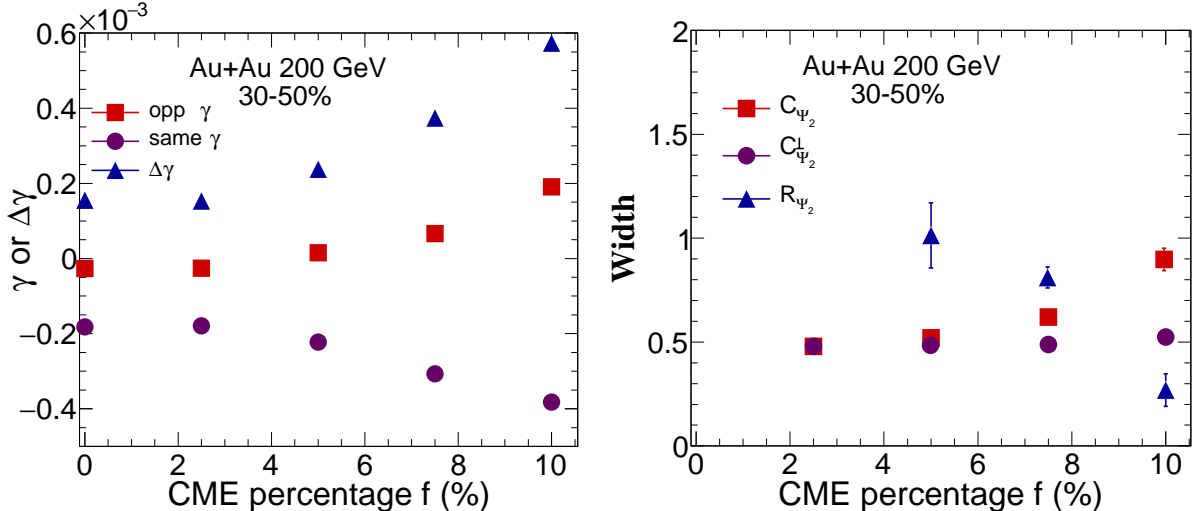


FIG. 6: (Color online) The initial charge separation percentage dependence of final  $\gamma$ ,  $\Delta\gamma$  (left plot), and the width of  $C_{\Psi_2}$ ,  $C_{\Psi_2}^\perp$  and  $R_{\Psi_2}$  (right plot) in Au+Au collisions at 200 GeV (30-50%).

both  $\gamma$  and  $R_{\Psi_2}$  start to be sensitive when the initial charge separation percentage become large enough (more than  $\sim 5\%$ ). But we should mention that the comparison may be unfair, because we are comparing the magnitude of  $\gamma$  with the shape of  $R_{\Psi_2}$  in term of their sensitivity to the CME.

#### IV. SUMMARY

We have studied the chiral magnetic effect with the new observable of  $R_{\Psi_m}$  within the framework of a multiphase transport model without and with introducing CME-induced charge separation. The results from mixing-particle method and shuffling-particle method are consistent with each other. We confirm that the shape of  $R_{\Psi_2}$  distribution is flat for the background only, while it can be concave if with some amount of CME, which reveals that  $R_{\Psi_2}$  is a good observable to distinguish the CME signal from the background. But for  $R_{\Psi_3}$ , it is not sensitive to the CME. We also presented the stage evolution of  $R_{\Psi_2}$  distribution, which indicates the initial CME signal will be weakened by strong final state interactions, similar as  $\gamma$ . We also compared the sensitivity to the CME between  $R_{\Psi_2}$  and  $\gamma$ , and found that both observables show nonlinear responses to the CME, which indicates the initial CME signal can survive from final state interactions only when the CME-induced charge separation percentage is large enough (more than  $\sim 5\%$ ).

#### ACKNOWLEDGMENTS

We thank Roy Lacey and Jiangyong Jia for their valuable discussions. This work was supported by the National Natural Science Foundation of China under Grants No. 11890714, No. 11835002, No. 11421505, No. 11522547 and No. 11375251, the Key Research Program of the Chinese Academy of Sciences under Grant No. XDPB09.

- 
- [1] J. Adams *et al.* [STAR Collaboration], Nucl. Phys. A **757**, 102 (2005) [nucl-ex/0501009].
  - [2] K. Adcox *et al.* [PHENIX Collaboration], Nucl. Phys. A **757**, 184 (2005) [nucl-ex/0410003].
  - [3] X. N. Wang and M. Gyulassy, Phys. Rev. Lett. **68**, 1480 (1992).
  - [4] J. Adams *et al.* [STAR Collaboration], Phys. Rev. Lett. **91**, 172302 (2003) [nucl-ex/0305015].
  - [5] K. Aamodt *et al.* [ALICE Collaboration], Phys. Lett. B **696**, 30 (2011) [arXiv:1012.1004 [nucl-ex]].
  - [6] J. Y. Ollitrault, Phys. Rev. D **46**, 229 (1992).
  - [7] P. Romatschke and U. Romatschke, Phys. Rev. Lett. **99**, 172301 (2007) [arXiv:0706.1522 [nucl-th]].
  - [8] U. Heinz and R. Snellings, Ann. Rev. Nucl. Part. Sci. **63**, 123 (2013) [arXiv:1301.2826 [nucl-th]].

- [9] Z. Xu, C. Greiner and H. Stoecker, Phys. Rev. Lett. **101**, 082302 (2008) [arXiv:0711.0961 [nucl-th]].
- [10] D. Kharzeev, Phys. Lett. B **633**, 260 (2006) [hep-ph/0406125].
- [11] D. Kharzeev and A. Zhitnitsky, Nucl. Phys. A **797**, 67 (2007) [arXiv:0706.1026 [hep-ph]].
- [12] D. E. Kharzeev, L. D. McLerran and H. J. Warringa, Nucl. Phys. A **803**, 227 (2008) [arXiv:0711.0950 [hep-ph]].
- [13] K. Fukushima, D. E. Kharzeev and H. J. Warringa, Phys. Rev. D **78**, 074033 (2008) [arXiv:0808.3382 [hep-ph]].
- [14] K. Fukushima, D. E. Kharzeev and H. J. Warringa, Nucl. Phys. A **836**, 311 (2010) [arXiv:0912.2961 [hep-ph]].
- [15] B. I. Abelev *et al.* [STAR Collaboration], Phys. Rev. Lett. **103**, 251601 (2009) [arXiv:0909.1739 [nucl-ex]].
- [16] B. I. Abelev *et al.* [STAR Collaboration], Phys. Rev. C **81**, 054908 (2010) [arXiv:0909.1717 [nucl-ex]].
- [17] B. Abelev *et al.* [ALICE Collaboration], Phys. Rev. Lett. **110**, no. 1, 012301 (2013) [arXiv:1207.0900 [nucl-ex]].
- [18] L. Adamczyk *et al.* [STAR Collaboration], Phys. Rev. C **88**, no. 6, 064911 (2013) [arXiv:1302.3802 [nucl-ex]].
- [19] L. Adamczyk *et al.* [STAR Collaboration], Phys. Rev. C **89**, no. 4, 044908 (2014) [arXiv:1303.0901 [nucl-ex]].
- [20] L. Adamczyk *et al.* [STAR Collaboration], Phys. Rev. Lett. **113**, 052302 (2014) [arXiv:1404.1433 [nucl-ex]].
- [21] V. Khachatryan *et al.* [CMS Collaboration], Phys. Rev. Lett. **118**, no. 12, 122301 (2017) [arXiv:1610.00263 [nucl-ex]].
- [22] S. Schlichting and S. Pratt, Phys. Rev. C **83**, 014913 (2011) [arXiv:1009.4283 [nucl-th]].
- [23] S. Pratt, S. Schlichting and S. Gavin, Phys. Rev. C **84**, 024909 (2011) [arXiv:1011.6053 [nucl-th]].
- [24] A. Bzdak, V. Koch, J. Liao, Phys. Rev. C **81** 031901 (2010), [arXiv:0912.5050 [nucl-th]].
- [25] A. Bzdak, V. Koch, J. Liao, Phys. Rev. C **83** 014905 (2011), [arXiv:1008.4919 [nucl-th]].
- [26] J. Liao, V. Koch, A. Bzdak, Phys. Rev. C **82** 054902 (2010), [arXiv:1005.5380 [nucl-th]].
- [27] F. Wang, Phys. Rev. C **81** 064902 (2010), [arXiv:0911.1482 [nucl-ex]].
- [28] A. Bzdak, V. Koch, J. Liao, Lect. Notes Phys. **871** 503 (2013), [arXiv:1207.7327 [nucl-th]].
- [29] J. Zhao, Z. Tu and F. Wang, Nucl. Phys. Rev. **35**, 225 (2018) [arXiv:1807.05083 [nucl-ex]].
- [30] N. N. Ajitanand, R. A. Lacey, A. Taranenko and J. M. Alexander, Phys. Rev. C **83**, 011901 (2011) [arXiv:1009.5624 [nucl-ex]].
- [31] N. Magdy, S. Shi, J. Liao, N. Ajitanand and R. A. Lacey, Phys. Rev. C **97**, no. 6, 061901 (2018) [arXiv:1710.01717 [physics.data-an]].
- [32] Y. Feng, J. Zhao and F. Wang, Phys. Rev. C **98**, no. 3, 034904 (2018) [arXiv:1803.02860 [nucl-th]].
- [33] P. Bozek, Phys. Rev. C **97**, no. 3, 034907 (2018) [arXiv:1711.02563 [nucl-th]].
- [34] V. Voronyuk, V. D. Toneev, W. Cassing, E. L. Bratkovskaya, V. P. Konchakovski and S. A. Voloshin, Phys. Rev. C **83**, 054911 (2011) [arXiv:1103.4239 [nucl-th]].
- [35] W. Cassing, O. Linnyk, T. Steinert and V. Ozvenchuk, Phys. Rev. Lett. **110**, no. 18, 182301 (2013) [arXiv:1302.0906 [hep-ph]].
- [36] H. T. Ding, F. Karsch and S. Mukherjee, Int. J. Mod. Phys. E **24**, no. 10, 1530007 (2015) [arXiv:1504.05274 [hep-lat]].
- [37] G. L. Ma, B. Zhang, Phys. Lett. B **700** 39 (2011), [arXiv:1101.1701 [nucl-th]].
- [38] Q. Y. Shou, G. L. Ma and Y. G. Ma, Phys. Rev. C **90**, no. 4, 047901 (2014) [arXiv:1405.2668 [nucl-th]].
- [39] L. Huang, C. W. Ma and G. L. Ma, Phys. Rev. C **97**, no. 3, 034909 (2018) [arXiv:1711.00637 [nucl-th]].
- [40] Z. W. Lin, C. M. Ko, B. A. Li, B. Zhang and S. Pal, Phys. Rev. C **72**, 064901 (2005) [nucl-th/0411110].
- [41] G. L. Ma and Z. W. Lin, Phys. Rev. C **93**, no. 5, 054911 (2016) [arXiv:1601.08160 [nucl-th]].
- [42] G. L. Ma, Phys. Rev. C **88**, no. 2, 021902 (2013) [arXiv:1306.1306 [nucl-th]].
- [43] G. L. Ma, Phys. Rev. C **89**, no. 2, 024902 (2014) [arXiv:1309.5555 [nucl-th]].
- [44] A. Bzdak and G. L. Ma, Phys. Rev. Lett. **113**, no. 25, 252301 (2014) [arXiv:1406.2804 [hep-ph]].
- [45] M. W. Nie, P. Huo, J. Jia and G. L. Ma, Phys. Rev. C **98**, no. 3, 034903 (2018) [arXiv:1802.00374 [hep-ph]].
- [46] X. N. Wang and M. Gyulassy, Phys. Rev. D **44**, 3501 (1991).
- [47] M. Gyulassy and X. N. Wang, Comput. Phys. Commun. **83**, 307 (1994) [nucl-th/9502021].
- [48] B. Zhang, Comput. Phys. Commun. **109**, 193 (1998) [nucl-th/9709009].
- [49] B. A. Li, C. M. Ko, Phys. Rev. C **52** 2037 (1995), [nucl-th/9505016].
- [50] G. L. Ma and X. N. Wang, Phys. Rev. Lett. **106**, 162301 (2011) [arXiv:1011.5249 [nucl-th]].